
Discovering mesoscopic descriptions of collective movement with neural stochastic modelling

Utkarsh Pratiush^{1,2} Arshed Nabeel^{3,4} Vishwesh Guttal³ Prathosh AP²

Abstract

Collective motion is an ubiquitous phenomenon in nature, inspiring engineers, physicists and mathematicians to develop mathematical models and bio-inspired designs. Collective motion at small to medium group sizes (~ 10 -1000 individuals, also called the ‘*mesoscale*’), can show nontrivial features due to stochasticity. Therefore, characterizing both the deterministic and stochastic aspects of the dynamics is crucial in the study of mesoscale collective phenomena. Here, we use a physics-inspired, neural-network based approach to characterize the stochastic group dynamics of interacting individuals, through a *stochastic differential equation (SDE)* that governs the collective dynamics of the group. We apply this technique on both synthetic and real-world datasets, and identify the deterministic and stochastic aspects of the dynamics using *drift* and *diffusion* fields, enabling us to make novel inferences about the nature of order in these systems.

1. Introduction

Collective motion is a phenomenon that is observed in natural and synthetic systems, and has fascinated physicists and biologists alike (Vicsek & Zafeiris, 2012; Sumpter, 2010; Camazine et al., 2020). Many systems across scales—such as microscopic organisms (Dinet et al., 2021; Be’er & Ariel, 2019), cells (Rørth, 2009; Alert & Trepat, 2020), human crowds (Chen et al., 2018b), and synthetic active matter (Ramaswamy, 2010; 2017)—exhibit self-organized collective movement. How the seemingly simple behaviour and interactions of the individuals give rise to the complex self-

organised emergent dynamics of the group, is one of the central questions in the study of collective dynamics.

At the level of individual organisms, animal behaviour is complex, and modelling every aspect of individual *stochastic* animal behaviour seems an unattainable goal. While the stochastic effects typically average out in the limit of infinite (or sufficiently large) group sizes, real-world animal groups are finite, and often small to medium sized (10 to 1000 individuals). At these ‘*mesoscopic*’ scales, the individual-level stochasticity can affect on the group dynamics in non-trivial ways. Therefore, a correct description of the dynamics at the mesoscale should incorporate stochasticity (McKane & Newman, 2004; Yates et al., 2009; Biancalani et al., 2014; Brückner et al., 2019; Jhavar et al., 2020).

Owing to the complexity at the individual behavioural level, one often uses a coarse-grained dynamical description of the collective system. A physicist’s way of approaching this is to quantify the state of the group, the so called *order parameter*, whose dynamics is then modelled to obtain a parsimonious description of the system. In the context of collective motion, order parameter can be the *group polarization*—a quantity analogous to the magnetisation of spin systems (Vicsek et al., 1995). To study the dynamics of order parameter at the mesoscale, the inherent stochasticity becomes crucial; and the order parameter dynamics must be modelled as a stochastic process. A commonly used framework for continuous stochastic processes such as this is the *diffusion process*, which can be described using a *stochastic differential equation (SDE)*. An SDE describes a stochastic process by disentangling it into a deterministic term, called the *drift*, and a stochastic term, called the *diffusion* (Van Kampen, 1992; Gardiner, 2009).

Analytically deriving coarse-grained SDE descriptions starting from individual-level interactions is an arduous task, even for highly simplified toy models of collective behaviour (McKane & Newman, 2004; Biancalani et al., 2014; Van Kampen, 1992; Jhavar et al., 2019). Indeed, for real-world collective systems, one seldom has a detailed understanding of the individual behaviour; therefore, obtaining a group-level description seems hopeless.

We address this challenge by tackling the inverse problem:

¹University of Tennessee, Knoxville, United States. ²Department of Electrical Communication Engineering, Indian Institute of Science, Bengaluru, India. ³Center for Ecological Sciences, Indian Institute of Science, Bengaluru, India. ⁴IISc Mathematics Initiative, Indian Institute of Science, Bengaluru, India.. Correspondence to: Vishwesh Guttal <guttal@iisc.ac.in>, Prathosh AP <prathosh@iisc.ac.in>.

we use a data-driven approach to estimate mesoscopic SDEs directly from observed group trajectory data. From the individual movement trajectories, we compute the *polarization order parameter*, quantifying the level of alignment in the group. We then use a physics-inspired, neural-network based approach (Dietrich et al., 2021; Evangelou et al., 2022) to fit an SDE model to describe the temporal dynamics of polarization. To facilitate the interpretability of the discovered neural SDE—something which is notoriously hard in neural-network-based approaches—we propose a method to visualize the discovered drift and diffusion as fields. The drift and diffusion fields enable us to readily identify the deterministic equilibria, structure of stochasticity, etc.

We use this approach to study both simulated as well as real-world fish (species *Etroplus suratensis*) schools. For a well-studied simulation model of collective behaviour (Buhl et al., 2006; Biancalani et al., 2014; Dyson et al., 2015; Jhavar et al., 2020; Jhavar & Guttal, 2020), the neural SDE models can accurately recover the mean field SDEs—and hence identify underlying interactions. We also discover SDEs from a real world dataset of schooling fish, where we observe the signatures of *noise-induced order*, a counter-intuitive phenomenon where intrinsic noise serves to increase group-level order rather than destroy it (Biancalani et al., 2014; Jhavar & Guttal, 2020). This was first observed by (Jhavar et al., 2020), who used the conventional SDE discovery methods (Jhavar & Guttal, 2020; Tabar, 2019). Our neural-network-based approach recapitulates the same result; we emphasize that this result is non-obvious, since neural SDEs capture a much wider hypothesis class than the conventional SDEs.

The main contributions of this study are as follows:

- We demonstrate the efficacy of neural-network-based approaches (Dietrich et al., 2021; Evangelou et al., 2022) for discovering mesoscale stochastic dynamics for collective behaviour data, using both simulated datasets where the mesoscale SDEs are analytically established.
- To make the results of the *grey-box* neural network techniques more interpretable, we propose novel visualization techniques to visualize the drift and diffusion fields in an easily interpretable form.
- We apply these techniques to study the mesoscale dynamics in real-world experimental datasets of fish schools (Jhavar et al., 2020), thereby demonstrating the significance of these techniques in animal behaviour and ecology. To the best of our knowledge, ours is the first study that applies these techniques to a real world dataset of animal collective behaviour, or even the broader field of ecology.

Related work: A class of techniques for estimating SDEs from data involve computing the *jump moments* from the observed time-series, and estimating the drift and diffusion coefficients of the SDE using certain conditional averages of the jump-moments (Tabar, 2019; Gardiner, 2009). However, these conditional averages are often noisy and inaccurate, especially when the available data is limited. More recently, approaches have been developed to use jump moments to obtain smooth estimates of the drift and diffusion coefficients, using kernel density estimation, sparse regression etc. (Gorjão & Meirinhos, 2019; Nabeel et al., 2022; Boninsegna et al., 2018; Wang et al., 2022). Another approach is to use parametric estimation techniques, by assuming an appropriate parametric form for the drift and diffusion functions (Nielsen et al., 2000)—however, these techniques have the drawback of having to know the parametric form of the SDE *a priori*.

The neural-network-based approach used in this study was first introduced by (Dietrich et al., 2021), and was subsequently applied to derive effective SDE descriptions from simulated Brownian dynamics (Evangelou et al., 2022). This is a *‘physics-inspired, grey-box’* approach, where partial knowledge and assumptions about the underlying physics is used to make the neural network model at least partly interpretable.

Alternative approaches for data-driven neural SDE modelling also exist in literature, such as (Song et al., 2020; Li et al., 2020), which build on previous work on neural ODEs (Chen et al., 2018a; Liu et al., 2020). Alternative approaches work by matching moments (O’Leary et al., 2021) or ensemble distributions (O’Leary et al., 2021), or use VAEs to learn an SDE in a latent space (Hasan et al., 2021). We chose the approach of (Dietrich et al., 2021) for its simplicity and flexibility because of the way the drift and diffusion are explicitly modelled and incorporated into a straightforward loss-function.

2. Background & Methods

2.1. Datasets

We use both simulated as well as real-world datasets of collective movement in this study. The simulated data comes from an idealized model of collective movement, for which the mesoscopic dynamics are well-studied (Jhavar et al., 2020; 2019). The real-world dataset is an open-access dataset ((Jhavar & Karichannawar, 2020)), consisting of trajectories of fish schools of different group sizes.

Agent based models for collective movement. We use simulations from an idealized agent based model of collective movement, with $N = 30$ individuals. Each individual is described solely by its velocity vector \mathbf{v}_i . The magnitude

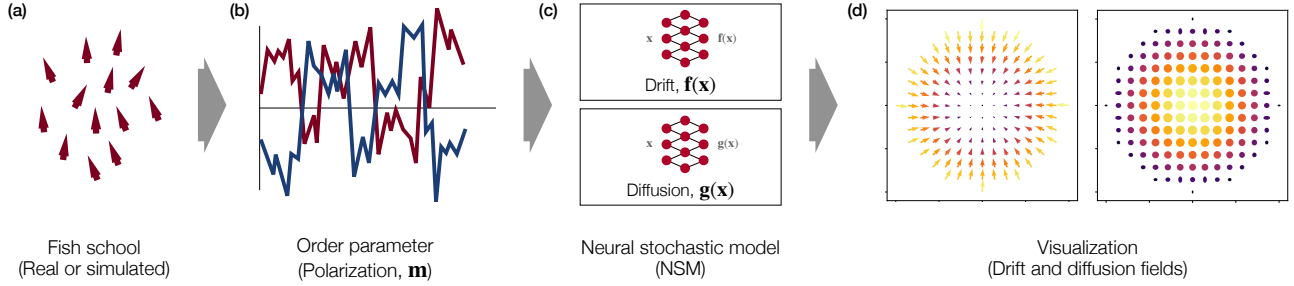


Figure 1. Schematic of the estimation procedure. (a) Individual trajectories are recorded for a real or simulated collective motion. (b) From the individual trajectories, the polarization order parameter (\mathbf{m}) is computed, quantifying the degree of alignment in the school. (c) Neural networks are trained, using a likelihood framework, to estimate the drift (\mathbf{f}) and diffusion (\mathbf{g}) functions. (d) For interpretation, the drift and diffusion functions are visualized as vector and tensor fields respectively. This figure shows a schematic illustration, see Section 2.5 and Fig. 3, 4.

of \mathbf{v}_i is assumed to be constant across all agents and across time, only the direction changes. Direction changes can happen asynchronously at random time-points, in one of two ways:

1. An agent i can spontaneously turn and choose a new direction, i.e. $\theta_i(t) \leftarrow \eta$ for $\eta \sim \text{Unif}[-\pi, +\pi]$.
2. An agent i can copy the direction of one or more other agents, chosen randomly from the entire group.

The turn and copy events themselves happen as a Poisson process. The models can be classified as *pairwise* or *ternary* interaction models based on how many neighbours are copied. The mesoscopic SDEs for these models are already known in literature (Jhawar et al., 2020; 2019)—also see Appendix A. Therefore, the model simulations act as a test-bed to verify the efficacy of the data-driven estimation procedure.

Real-world datasets of schooling fish. We used an openly available dataset of fish schooling (Jhawar et al., 2020; Jhawar & Karichannawar, 2020). This dataset consists of the position $\mathbf{x}_i(t)$ and velocity $\mathbf{v}_i(t)$ trajectories of fish (species *Etroplus suratensis*), swimming in a circular arena. From the individual fish trajectories, the polarization order parameter is computed as detailed in the following section. We used datasets with $N = 15, 30$ and 60 fish. The data was available at a sampling interval of $0.12s$.

2.2. Mesoscopic descriptions of collective dynamics

While modelling collective movement, the emergent dynamics of the group can often be characterized in terms of an *order parameter*, which characterizes the degree of order in the group. An oft-used order parameter is the group polarization, which captures the level of alignment among the individuals of the group.

For a group of N individuals, each with positions \mathbf{x}_i and velocities \mathbf{v}_i , the polarization can be computed as the mean of the normalized velocity vectors, i.e.,

$$\mathbf{m} = \frac{1}{N} \sum_{i=1}^N \frac{\mathbf{v}_i}{|\mathbf{v}_i|} \quad (1)$$

Modelling the time-evolution of \mathbf{m} allows us to gain an understanding of the overall emergent dynamics of the group. For relatively small group sizes, idiosyncrasies in the individual \mathbf{v}_i 's can have a significant effect on the group dynamics. These result in stochastic fluctuations which cannot be ignored while modelling the dynamics of \mathbf{m} . Therefore, we use the framework of *stochastic differential equations (SDE)* to model the \mathbf{m} , which models both deterministic as well as stochastic aspects of the time-evolution of \mathbf{m} .

2.3. Data-driven discovery of stochastic differential equations

Given the time series of the 2-dimensional polarization vector $\mathbf{m}(t)$ sampled with a finite time-interval Δt , our goal is to discover an Itô stochastic differential equation (SDE) model that explains the time-series, of the following form:

$$\frac{d\mathbf{m}}{dt} = \mathbf{f}(\mathbf{m}) + \mathbf{g}(\mathbf{m}) \cdot \boldsymbol{\eta}(t) \quad (2)$$

where $\boldsymbol{\eta}$ is 2-dimensional white noise process. Here, \mathbf{f} is called the *drift* function and \mathbf{g} is called the *diffusion* function. The goal in the SDE discovery problem is to discover representations for \mathbf{f} and \mathbf{g} . In this work, we use a likelihood-based framework, first introduced by (Dietrich et al., 2021). Here, \mathbf{f} and \mathbf{g} are represented using neural networks, trained to maximize a likelihood function based on the finite-time transition probability.

Specifically, let $p(\cdot, t_1 | \mathbf{m}_0, t_0)$ be the probability density function of $\mathbf{m}(t_1)$ conditional to $\mathbf{m}(t_0) = \mathbf{m}_0$. Then, for a small time-step Δt , $p(\cdot, t + \Delta t | \mathbf{m}_0, t)$ can be approximated based on the stochastic Euler approximation (also known as the Euler Maruyama approximation) as:

$$p(\cdot, t + \Delta t | \mathbf{m}_0, t) \sim \mathcal{N}(\mathbf{m}_0 + \mathbf{f}(\mathbf{m}_0) \cdot \Delta t, \mathbf{g}(\mathbf{m}_0) \cdot \Delta t) \quad (3)$$

Parameterizing p in terms of the drift and diffusion functions as $p_{\mathbf{f}, \mathbf{g}}$, this gives rise to the following log-likelihood loss function which can be maximized to fit \mathbf{f} and \mathbf{g} :

$$\begin{aligned} \mathcal{L}(\mathbf{f}, \mathbf{g} | \mathbf{m}_0, \mathbf{m}_1) &= \log p_{\mathbf{f}, \mathbf{g}}(\mathbf{m}_1, t + \Delta t | \mathbf{m}_0, t) \\ &= \frac{(\mathbf{m}_1 - \mathbf{m}_0 - \mathbf{f}(\mathbf{m}_0)\Delta t)^2}{\mathbf{g}(\mathbf{m}_0)^2 \Delta t} + \log |\mathbf{g}(\mathbf{m}_0)^2 \Delta t| + \log 2\pi \end{aligned} \quad (4)$$

where \mathbf{m}_0 and \mathbf{m}_1 are successive points in the time series dataset, sampled Δt apart. The loss function \mathcal{L} can be minimized to fit an appropriate representation of \mathbf{f} and \mathbf{g} .

We represent \mathbf{f} and \mathbf{g} using neural networks, which were trained to minimize the loss function in Equation 4—see Section 2.4 for further details about the implementation. Figure 1 illustrates the full data-driven model discovery procedure, starting from the individual trajectories, computing the polarization order parameter, estimating drift and diffusion using neural networks, and visualizing them as fields.

2.4. Implementation details

Dataset preparation: The agent-based schooling model was implemented and simulated in MATLAB, using the stochastic simulation algorithm (SSA) (Gillespie et al., 2007). From the trajectories of individual velocity vectors produced by the simulation, the group polarization $\mathbf{m}(t)$ was computed (Section 2.2), which was used for training the model. Similarly, for the fish schooling dataset, the tracked individual trajectories (see Section 2.1) were used to compute the group polarization $\mathbf{m}(t)$.

In both the agent-based models as well as real-world datasets, there is rotational and mirror symmetry in the dynamics (the simulations has no angular bias, while the fish schools were swimming in a circular arena). Therefore, we expect these symmetries to carry over to the mean-field models as well. To encourage the neural network to learn these symmetries, we augment the time-series of $\mathbf{m}(t)$ with rotated (16 rotations equally spaced between $-\pi$ and π) and flipped (horizontal and vertical flips) versions of itself.

Architecture and training details: The drift and diffusion functions \mathbf{f} and \mathbf{g} were represented using fully-connected neural networks with 5 layers and 150 neurons per layer, with ELU activation function (Clevert et al., 2015). The network was trained with a batch size 512 and test-train split of 90:10, with the Adamax optimizer.

Once the models are trained, to validate the discovered models, we generate simulated trajectories using the model, and compare the probability density (histogram) and autocorrelation function of the simulated trajectory to that of the input trajectory. The similarity between the histograms was quantified using the Wasserstein metric, W_1 (Ramdas et al., 2017). The similarity of the autocorrelation was quantified using the relative timescale discrepancy, $T_{\text{rel}} = |\tau - \hat{\tau}|/\tau$, where τ and $\hat{\tau}$ are the autocorrelation times of the real and simulated time series respectively. A good fit according to these metrics ensures that the discovered dynamical model matches the actual dynamics at least in the weak (distributional) sense (Kloeden et al., 1992).

2.5. Visualizing the drift and diffusion fields

Since the drift and diffusion functions are represented as neural networks (and not equations that are immediately interpretable), a proper visualization is crucial to enable easy interpretation of the discovered dynamical model. To do this, we visualize the drift and diffusion functions as fields.

Visualizing \mathbf{f} is relatively straightforward. Since $\mathbf{f} : \mathbb{R}^2 \rightarrow \mathbb{R}^2$ is a vector function, it can be visualized as a vector field—see Figure 3 (a) for an example. The arrows indicate the strength and direction of the drift field at each value of \mathbf{m} . The vector field representation makes it easy to identify features equilibrium points (the vectors will have zero length at the equilibrium point) and their stability (near an equilibrium point, the vectors will point towards it if it is stable, and away from it if it is unstable).

Visualizing the diffusion field is more intricate: since $\mathbf{g} : \mathbb{R}^2 \rightarrow \mathbb{R}^{2 \times 2}$ is a matrix function, the diffusion field is a tensor field. First, notice that for a given \mathbf{m} , the covariance matrix of \mathbf{m} is given by $G(\mathbf{m}) = \mathbf{g}(\mathbf{m})\mathbf{g}(\mathbf{m})^T$. For any value of \mathbf{m} , $G(\mathbf{m})$ can be represented by an ellipse centered at \mathbf{m} , with its axes parallel to the eigenvectors of $G(\mathbf{m})$ and axis lengths proportional to the eigenvalues of $G(\mathbf{m})$. This is a representation of the diffusion tensor field, and gives an overview of the strength and directionality of the diffusive force for each value of \mathbf{m} . For readers familiar with tensor field visualizations, this is a visualization of the G -tensor with elliptical glyphs.

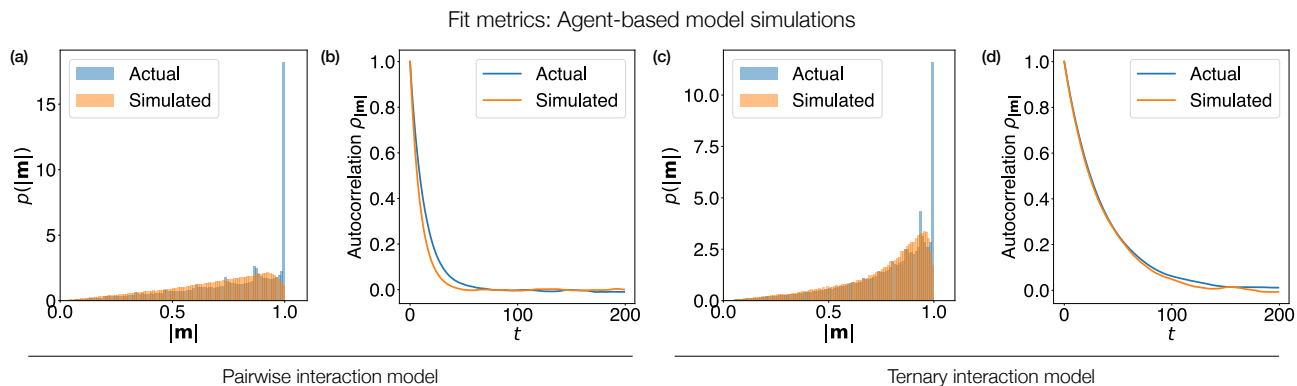


Figure 2. Goodness-of-fit metrics for mesoscale models for agent-based simulations. (a, c) Comparison of histograms of $|\mathbf{m}|$ from the actual time series as well as a time series simulated with the discovered neural stochastic model; for the pairwise (a) and ternary (c) interaction models. (b, d) A similar comparison between the autocorrelation functions of the actual and simulated $|\mathbf{m}|$ time series from the two models.

3. Results

3.1. Mesoscopic equations for simulation models of collective behaviour

We first used our approach to discover the mesoscopic dynamics from simulated trajectories, for a class of models where the mesoscopic SDEs are already known—see Section 2.1. This serves as a test-bed for the efficacy of the approach. With pairwise as well as ternary interactions, the simulated flocks show a high degree of polarization. However, the mechanism by which order is created is fundamentally different in these two models.

Figure 2 compares the histogram and autocorrelation of a simulated time series from the discovered models, to that of the input time series used to train the model (also see Table 1). There is a close match between the input and the generated data (*pairwise*: $W_1 = 0.0686$, $T_{\text{rel}} = 0.2770$, *ternary*: $W_1 = 0.0270$, $T_{\text{rel}} = 0.0437$). We emphasize that this is despite the model not being directly trained to match the histogram or the autocorrelation—suggesting that the discovered models are good approximations for the actual mesoscopic dynamics.

The estimated drift and diffusion fields are shown in Figure 3. For a model with pairwise interactions, the drift field shows a single attractor at the origin, denoting that the deterministic dynamics has the effect of depolarising the group. However, the strength of diffusion is maximum at the origin and decreases as $|\mathbf{m}|$: this means that the stochastic forces push the system away from the $\mathbf{m} = 0$ stable state, creating order in the system. This counter-intuitive phenomenon of high polarisation arising as a consequence of stochastic effects is called *noise induced order* in literature.

Contrast this with the case of the ternary interaction model,

where the drift field shows ring-shaped attractor, at a high value of $|\mathbf{m}|$. The diffusion field is similar to the pairwise model, with diffusion being strongest near the origin and decreasing outwards. This means that the order in the ternary interaction model is primarily deterministic.

This demonstrates that our approach is able to distinguish between the fundamentally different dynamics in the two models considered, despite the time series and the histogram of the datasets looking qualitatively similar. Indeed, the estimated models are also in qualitative agreement with theoretical predictions (Appendix A).

3.2. Mesoscopic equations for real-world fish schools

We now move on to modelling the stochastic mesoscopic dynamics of a real-world data set of collective motion, based on a recently published dataset on schools of fish (Jhawar et al., 2020). Similar to the simulation models, we seek to discover mesoscopic SDEs for the dynamics of the polarization order-parameter \mathbf{m} of real schools of fish.

We observe that the deterministic mean-field dynamics of the school, characterized by the drift field, drives the system towards a disordered state ($\mathbf{m} = 0$). However, the diffusion is maximum at $\mathbf{m} = 0$, driving the system away from the stable state and resulting in noise induced order, similar to the model system with pairwise interactions. This surprising phenomenon was first observed in real-world fish schools in (Jhawar et al., 2020); our neural approach is able to reproduce this result. This is a non-trivial result: despite the neural networks being able to represent a much larger hypothesis class, the drift and diffusion fields converged to the simple forms shown in Figure 4.

We also derived mesoscopic models for fish schools of group

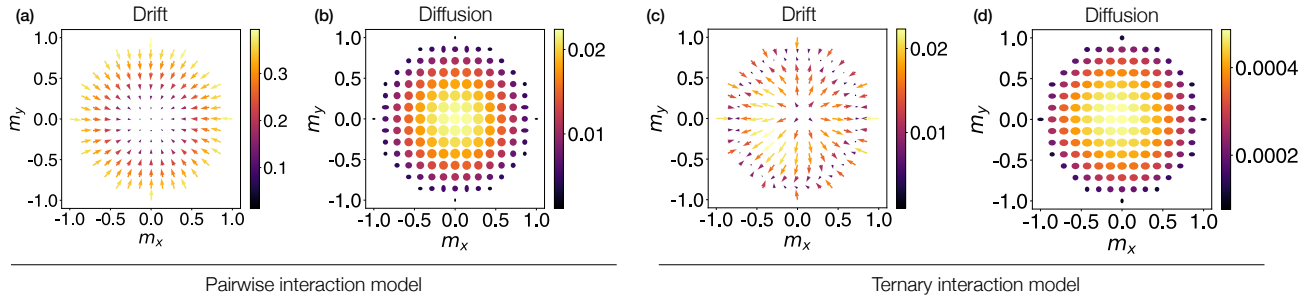


Figure 3. Mesoscopic dynamics of simulated fish schools. The drift and diffusion fields estimated by the neural model agree with the theoretically predicted drift and diffusion fields. (a) Drift field for a simulated school with only pairwise interactions, showing a single attractor at $\mathbf{m} = 0$. (b) Diffusion field for the pairwise model simulation, showing that the strength of diffusion is maximum at $\mathbf{m} = 0$ and decreases outwards. (c) Drift field for a simulated school with higher-order (ternary) interactions, showing a ring-shaped attractor for a high value of $|\mathbf{m}|$. (d) Diffusion field for the ternary model simulation, showing the same pattern of diffusion as in the pairwise model.

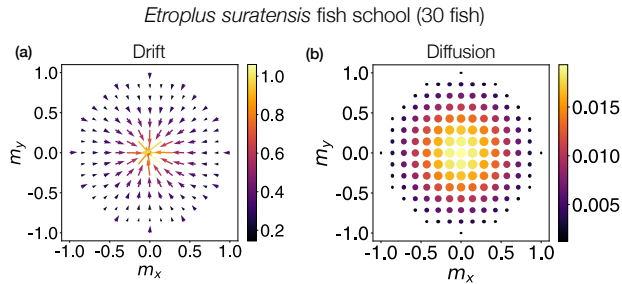


Figure 4. Mesoscopic dynamics of a real-world school of 30 *Etroplus suratensis* fish. The observed drift and diffusion fields show evidence for noise-induced order. (a) Drift field for the *Etroplus* school, showing a single attractor at $\mathbf{m} = 0$. (b) Diffusion field for school, showing that the strength of diffusion is maximum at $\mathbf{m} = 0$ and decreases outwards.

sizes 15 and 60. The results are described in Appendix B and Figure 7, and are qualitatively similar to the results for the 30-fish school. The net strength of diffusion goes down as the school size increases, an observation that matches theoretical predictions (Appendix A).

The fit metrics for the fish schooling dataset (30 fish) is shown in Figure 5 (also see Table 1). Like the agent-based models, there is a good agreement between the histograms of the actual and the simulated $|\mathbf{m}|$ time series ($W_1 = 0.0823$). However, autocorrelation function shows a deviation from the actual time-series ($T_{\text{rel}} = 0.6652$). This deviation is present in other group sizes also (15 and 60 fish). This deviation is because of a spurious periodicity in the time series of $|\mathbf{m}|$ —caused by the fish swimming along the boundary of the tank—which is not captured by the mesoscopic SDE model. The deviation is also present with other SDE estimation techniques (see Table 1), and is a constraint of the model itself, and not the estimation procedure.

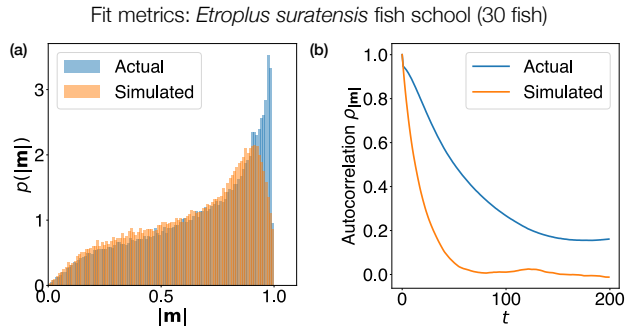


Figure 5. Goodness-of-fit metrics for mesoscale models for a real-world fish school. (a) Comparison of histograms of $|\mathbf{m}|$ from the actual time series as well as a time series simulated with the discovered neural stochastic model; for the schooling dynamics of a school of 30 fish. (b) Comparison of the autocorrelation functions between the real and simulated time series for the same dataset.

Table 1 summarizes the quantitative performance of the neural effective SDE estimation technique, on the five different datasets considered in this study (2 simulated agent-based models, 3 real-world fish schools of different sizes). For comparison, we use a package PyDaDDy (Nabeel et al., 2022), which estimates SDEs from data using classical techniques, *viz.* jump-moment estimation and equation-learning with sparse-regression. While we reemphasize that the focus of a study like this is to obtain interpretable models; overall, the neural SDE estimation approach performs quantitatively better than PyDaddy, in both the Wasserstein metric W_1 and relative timescale discrepancy T_{rel} .

4. Discussion

Compared to conventional techniques for SDE identification, neural networks have the advantage of being less restrictive

Table 1. Comparison of model performance with a classical technique for data-driven SDE discovery

Dataset	Neural SDE		PyDaddy	
	W_1	T_{rel}	W_1	T_{rel}
ABM (Pairwise)	0.0686	0.2770	0.767	0.3020
ABM (Ternary)	0.0270	0.0437	0.0283	0.1583
Etroplus (15 fish)	0.0823	0.6652	0.0818	0.7787
Etroplus (30 fish)	0.0357	0.5895	0.0263	0.7144
Etroplus (60 fish)	0.0155	0.2217	0.0302	0.4409

in the hypothesis space they encompass, and hence are more general. It is worth noting that, even with the added flexibility, the neural approach still discovers qualitatively the same model for fish schools as (Jhawar et al., 2020), lending further credence to the observation of noise-induced order in the original study.

Indeed, we expect the neural-network based approach to be more powerful—even necessary—in scenarios with more complex movement, which lack these symmetries. For example, organisms could be moving under the influence of an inhomogeneous light or chemical field (Tian et al., 2021; Puckett et al., 2018). In such cases, enforcing user-defined parametric models, or relying on simple hypothesis classes (such as polynomials), may impose strong and often undesirable inductive biases on the SDE discovery process, which the neural-net-based approach avoids.

Further, the likelihood-based estimation procedure is readily generalizable to more complex stochastic dynamics. While such extensions are out of the scope of the current work, it is worth highlighting that the framework is quite general, and can be extended to accommodate jump discontinuities, extrinsic driver variables, non-stationarity, etc., all of which are commonly observed in real-world datasets (Carpenter et al., 2020; Salmaso, 2000).

Finally, we emphasize the need for proper visualization tools to facilitate interpretability of the discovered models. When the goal of model discovery is scientific inquiry (and not merely to obtain a predictive model), tools to interpret and analyze the discovered models become crucial. Our proposed way of visualizing the drift and diffusion fields achieves exactly this, and enables one to easily understand the deterministic phase portrait and the stochasticity landscape of the discovered model.

5. Conclusion

In this study, we utilize a physics-informed, grey-box neural network model to discover mesoscale SDEs for collective movement (Dietrich et al., 2021; Evangelou et al., 2022). Using this technique, we discover SDEs for both simulated

and real-world datasets of collective movement. With simulated datasets, this approach is able to identify the difference between different models, even when the time series and histograms look qualitatively similar. Furthermore, the SDEs discovered by this approach in each case are qualitatively similar to the ones predicted by theory. For a real-world dataset of schooling fish, the neural-net approach discovers an SDE that predicts *noise-induced order*, reproducing the result of a recent study (Jhawar et al., 2020) that used conventional SDE estimation techniques.

To conclude, we demonstrate the applicability and versatility of neural network models for studying stochastic dynamics of collective animal movement, and of biological systems in general. The combination of a physics-informed, grey-box estimation process along with proper visualization techniques enabled us to discover models that are quantitatively more accurate than traditional approaches (Table 1), while still remaining readily interpretable. As high-quality datasets of complex phenomena become commonplace in biology and related fields, these techniques—and clear ways to interpret them—become indispensable.

Code & Data Availability

The fish schooling dataset used in this study is an openly available dataset, available at (Jhawar & Karichannawar, 2020).

The neural SDE identification code was a modified version of (Dietrich, 2021). Our modified version of the code is available at https://github.com/utkarshp1161/Neu_sde.

Acknowledgements

We thank Vivek Jadhav for his help with the agent-based model simulations, and Somaditya Santra for discussions. P. A. P. acknowledges funding from the Infosys foundation.

References

- Alert, R. and Trepast, X. Physical models of collective cell migration. *Annual Review of Condensed Matter Physics*, 11:77–101, 2020.
- Be’er, A. and Ariel, G. A statistical physics view of swarming bacteria. *Movement ecology*, 7(1):1–17, 2019.
- Biancalani, T., Dyson, L., and McKane, A. J. Noise-induced bistable states and their mean switching time in foraging colonies. *Physical review letters*, 112(3):038101, 2014.
- Boninsegna, L., Nüske, F., and Clementi, C. Sparse learning of stochastic dynamic equations. *The Journal of Chemical Physics*, 148(24):241723, June 2018. ISSN 0021-9606, 1089-7690. doi: 10.1063/1.5018409. URL

- <http://arxiv.org/abs/1712.02432>. arXiv: 1712.02432.
- Brückner, D. B., Fink, A., Schreiber, C., Röttgermann, P. J., Rädler, J. O., and Broedersz, C. P. Stochastic nonlinear dynamics of confined cell migration in two-state systems. *Nature Physics*, 15(6):595–601, 2019.
- Buhl, J., Sumpter, D. J., Couzin, I. D., Hale, J. J., Despland, E., Miller, E. R., and Simpson, S. J. From disorder to order in marching locusts. *Science*, 312(5778):1402–1406, 2006.
- Camazine, S., Deneubourg, J.-L., Franks, N. R., Sneyd, J., Theraula, G., and Bonabeau, E. Self-organization in biological systems. In *Self-Organization in Biological Systems*. Princeton university press, 2020.
- Carpenter, S. R., Arani, B. M., Hanson, P. C., Scheffer, M., Stanley, E. H., and Van Nes, E. Stochastic dynamics of cyanobacteria in long-term high-frequency observations of a eutrophic lake. *Limnology and Oceanography Letters*, 5(5):331–336, 2020.
- Chen, R. T., Rubanova, Y., Bettencourt, J., and Duvenaud, D. K. Neural ordinary differential equations. *Advances in neural information processing systems*, 31, 2018a.
- Chen, X., Treiber, M., Kanagaraj, V., and Li, H. Social force models for pedestrian traffic—state of the art. *Transport reviews*, 38(5):625–653, 2018b.
- Clevert, D.-A., Unterthiner, T., and Hochreiter, S. Fast and accurate deep network learning by exponential linear units (elus). *arXiv preprint arXiv:1511.07289*, 2015.
- Dietrich, F. SDE Identification. <https://gitlab.com/felix.dietrich/sde-identification>, 2021.
- Dietrich, F., Makeev, A., Kevrekidis, G., Evangelou, N., Bertalan, T., Reich, S., and Kevrekidis, I. G. Learning effective stochastic differential equations from microscopic simulations: combining stochastic numerics and deep learning. *arXiv:2106.09004 [physics]*, 2021. URL <http://arxiv.org/abs/2106.09004>. arXiv: 2106.09004.
- Dinet, C., Michelot, A., Herrou, J., and Mignot, T. Linking single-cell decisions to collective behaviours in social bacteria. *Philosophical Transactions of the Royal Society B*, 376(1820):20190755, 2021.
- Dyson, L., Yates, C. A., Buhl, J., and McKane, A. J. Onset of collective motion in locusts is captured by a minimal model. *Physical Review E*, 92(5):052708, 2015.
- Evangelou, N., Dietrich, F., Bello-Rivas, J. M., Yeh, A., Stein, R., Bevan, M. A., and Kevekidis, I. G. Learning Effective SDEs from Brownian Dynamics Simulations of Colloidal Particles. *arXiv:2205.00286 [cs, math]*, April 2022. URL <http://arxiv.org/abs/2205.00286>. arXiv: 2205.00286.
- Gardiner, C. *Stochastic methods*, volume 4. springer Berlin, 2009.
- Gillespie, D. T. et al. Stochastic simulation of chemical kinetics. *Annual review of physical chemistry*, 58(1): 35–55, 2007.
- Gorjão, L. R. and Meirinhos, F. kramersmoyal: Kramers–moyal coefficients for stochastic processes. *Journal of Open Source Software*, 4(44):1693, 2019.
- Hasan, A., Pereira, J. M., Farsiu, S., and Tarokh, V. Identifying latent stochastic differential equations. *IEEE Transactions on Signal Processing*, 70:89–104, 2021.
- Jhavar, J. and Guttal, V. Noise-induced effects in collective dynamics and inferring local interactions from data. *Philosophical Transactions of the Royal Society B*, 375 (1807):20190381, 2020.
- Jhavar, J. and Karichannawar, A. tee-lab/schooling_fish, January 2020. URL <https://doi.org/10.5281/zenodo.3632470>.
- Jhavar, J., Morris, R. G., and Guttal, V. Deriving Mesoscopic Models of Collective Behavior for Finite Populations. In *Handbook of Statistics*, volume 40, pp. 551–594. Elsevier, 2019. ISBN 978-0-444-64152-6. doi: 10.1016/bs.host.2018.10.002.
- Jhavar, J., Morris, R. G., Amith-Kumar, U., Danny Raj, M., Rogers, T., Rajendran, H., and Guttal, V. Noise-induced schooling of fish. *Nature Physics*, 16(4):488–493, 2020.
- Kloeden, P. E., Platen, E., Kloeden, P. E., and Platen, E. *Stochastic differential equations*. Springer, 1992.
- Li, X., Wong, T.-K. L., Chen, R. T., and Duvenaud, D. Scalable gradients for stochastic differential equations. In *International Conference on Artificial Intelligence and Statistics*, pp. 3870–3882. PMLR, 2020.
- Liu, J., Long, Z., Wang, R., Sun, J., and Dong, B. Rode-net: learning ordinary differential equations with randomness from data. *arXiv preprint arXiv:2006.02377*, 2020.
- McKane, A. J. and Newman, T. J. Stochastic models in population biology and their deterministic analogs. *Physical Review E*, 70(4):041902, 2004.

- Nabeel, A., Karichannavar, A., Palathingal, S., Jhavar, J., Danny Raj, M., and Guttal, V. Pydaddy: A python package for discovering stochastic dynamical equations from timeseries data. *arXiv preprint arXiv:2205.02645*, 2022.
- Nielsen, J. N., Madsen, H., and Young, P. C. Parameter estimation in stochastic differential equations: an overview. *Annual Reviews in Control*, 24:83–94, 2000.
- O’Leary, J., Paulson, J. A., and Mesbah, A. Stochastic physics-informed neural networks (spinn): A moment-matching framework for learning hidden physics within stochastic differential equations. *arXiv preprint arXiv:2109.01621*, 2021.
- Puckett, J. G., Pokhrel, A. R., and Giannini, J. A. Collective gradient sensing in fish schools. *Scientific reports*, 8(1): 1–11, 2018.
- Ramaswamy, S. The mechanics and statistics of active matter. *Annual Review of Condensed Matter Physics*, 1(1):323–345, 2010. doi: 10.1146/annurev-conmatphys-070909-104101. URL <https://doi.org/10.1146/annurev-conmatphys-070909-104101>.
- Ramaswamy, S. Active matter. *Journal of Statistical Mechanics: Theory and Experiment*, 2017(5):054002, 2017.
- Ramdas, A., García Trillos, N., and Cuturi, M. On wasserstein two-sample testing and related families of nonparametric tests. *Entropy*, 19(2):47, 2017.
- Rørth, P. Collective cell migration. *Annual Review of Cell and Developmental Biology*, 25:407–429, 2009.
- Salmaso, N. Factors affecting the seasonality and distribution of cyanobacteria and chlorophytes: a case study from the large lakes south of the alps, with special reference to lake garda. *Hydrobiologia*, 438(1):43–63, 2000.
- Song, Y., Sohl-Dickstein, J., Kingma, D. P., Kumar, A., Ermon, S., and Poole, B. Score-based generative modeling through stochastic differential equations. *arXiv preprint arXiv:2011.13456*, 2020.
- Sumpter, D. J. Collective animal behavior. In *Collective Animal Behavior*. Princeton University Press, 2010.
- Tabar, R. *Analysis and data-based reconstruction of complex nonlinear dynamical systems*, volume 730. Springer, 2019.
- Tian, M., Zhang, C., Zhang, R., and Yuan, J. Collective motion enhances chemotaxis in a two-dimensional bacterial swarm. *Biophysical journal*, 120(9):1615–1624, 2021.
- Van Kampen, N. G. *Stochastic processes in physics and chemistry*, volume 1. Elsevier, 1992.
- Vicsek, T. and Zafeiris, A. Collective motion. *Physics reports*, 517(3-4):71–140, 2012.
- Vicsek, T., Czirók, A., Ben-Jacob, E., Cohen, I., and Shochet, O. Novel Type of Phase Transition in a System of Self-Driven Particles. *Physical Review Letters*, 75(6):1226–1229, August 1995. ISSN 0031-9007, 1079-7114. doi: 10.1103/PhysRevLett.75.1226. URL <https://link.aps.org/doi/10.1103/PhysRevLett.75.1226>.
- Wang, Y., Fang, H., Jin, J., Ma, G., He, X., Dai, X., Yue, Z., Cheng, C., Zhang, H.-T., Pu, D., et al. Data-driven discovery of stochastic differential equations. *Engineering*, 2022.
- Yates, C. A., Erban, R., Escudero, C., Couzin, I. D., Buhl, J., Kevrekidis, I. G., Maini, P. K., and Sumpter, D. J. T. Inherent noise can facilitate coherence in collective swarm motion. *Proceedings of the National Academy of Sciences*, 106(14):5464–5469, April 2009. ISSN 0027-8424, 1091-6490. doi: 10.1073/pnas.0811195106. URL <https://pnas.org/doi/full/10.1073/pnas.0811195106>.

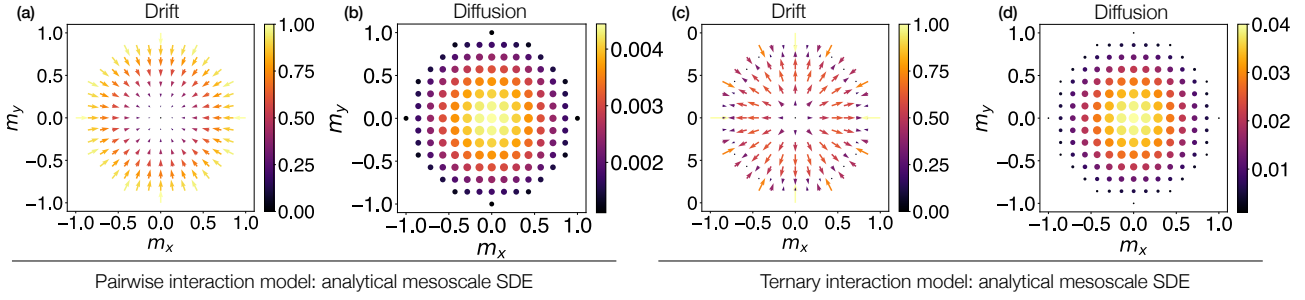


Figure 6. Analytically derived mesoscale dynamics of agent based models. (a) Analytically derived drift field for a model with only pairwise interactions, showing a single attractor at $\mathbf{m} = 0$. (b) Analytically derived diffusion field for the pairwise model, showing that the strength of diffusion is maximum at $\mathbf{m} = 0$ and decreases outwards. (c) Analytically derived drift field for a model with higher-order (ternary) interactions, showing a ring-shaped attractor for a high value of $|\mathbf{m}|$. (d) Analytically derived diffusion field for the ternary model simulation, showing the same pattern of diffusion as in the pairwise model.

A. Analytically derived mesoscopic SDEs for agent-based models

The agent-based models of collective behaviour used in this study have been well-studied, and mesoscopic SDEs for these models have been analytically derived (Jhavar et al., 2019; 2020).

Recap the model description:

- An agent i can spontaneously turn and choose a new direction, i.e. $\theta_i(t) \rightarrow \eta$ for $\eta \sim \text{Unif}[-\pi, \pi)$. The spontaneous turns happen as a Poisson process with a rate r_1 .
- An agent i can copy the direction of one (pairwise interaction) or the average direction of two (ternary interaction) other agents, chosen randomly from the group. The copy interactions can happen at rates r_2 and r_3 respectively.

For the pairwise interaction model, the mesoscale SDE can be analytically derived to be of the following form:

$$\frac{d\mathbf{m}}{dt} = -r_1 \mathbf{m} + \sqrt{\frac{r_1 + r_2 (1 - |\mathbf{m}|^2)}{N}} I \cdot \boldsymbol{\eta}(t) \quad (5)$$

where N is the total number of agents in the group.

Similarly, for the ternary interaction model, the derived mesoscale SDE has the form:

$$\frac{d\mathbf{m}}{dt} = -r_1 \mathbf{m} + r_3 (1 - |\mathbf{m}|^2) \mathbf{m} + \sqrt{\frac{r_1 + (r_2 + r_3) (1 - |\mathbf{m}|^2)}{N}} I \cdot \boldsymbol{\eta}(t) \quad (6)$$

The diffusion term is a diagonal matrix, and has a $1 - |\mathbf{m}|^2$ term. This means that the noise is maximum at $|\mathbf{m}| = 0$ and decreases with increasing $|\mathbf{m}|$. The drift term is linear in \mathbf{m} for the pairwise interaction model, and the deterministic stable equilibrium for this system is at $|\mathbf{m}| = 0$. Therefore, the order in the pairwise interaction model is noise-induced, and arises solely due to the high strength of diffusion near $|\mathbf{m}| = 0$. On the other hand, for the ternary interaction model, drift term is cubic in \mathbf{m} , and has a $(1 - |\mathbf{m}|^2) \mathbf{m}$ term. This contributes to a ring-shaped attractor near $|\mathbf{m}| = 1$, i.e. the order in the ternary interaction model originates from a combination of both deterministic and noise-induced effects.

The drift and diffusion fields generated from equations 5 and 6 are shown in Figure 6. There is a close correspondence between these plots and the ones in Figure 3, suggesting that the neural effective SDE approach is able to correctly infer the underlying mesoscale SDEs.

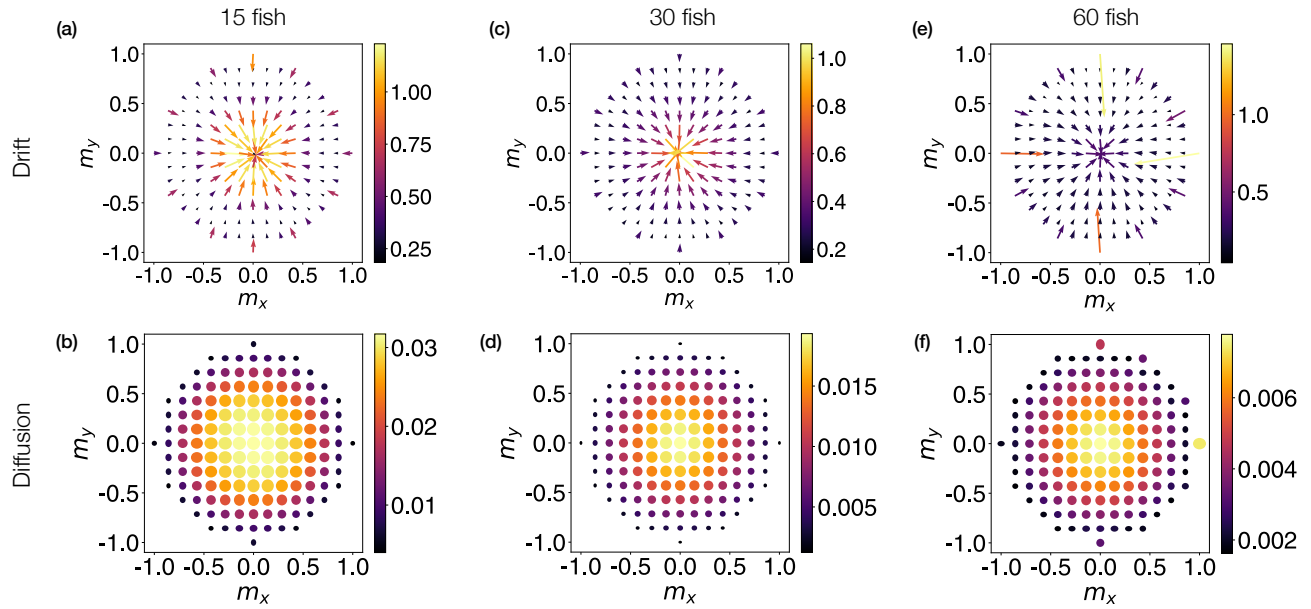


Figure 7. Estimated drift and diffusion fields for polarization dynamics of fish schools of different group sizes. (a, b) Drift and diffusion fields for \mathbf{m} for a 15-fish school (c, d) Drift and diffusion fields for \mathbf{m} for a 15-fish school, same as in Figure 4. (e, f) Drift and diffusion fields for \mathbf{m} for a 60-fish school.

B. Mesoscopic models for fish schools of different group sizes

We repeated the analysis in Section 3.2 on two other group sizes, *viz.* $N = 15$ and $N = 60$. The fit metrics and drift/diffusion fields are shown in Figure 7. Overall, the fields look qualitatively similar across different group sizes. However, the net strength of diffusion decreases with increasing group size (notice the range of the color axis). This is in accordance with theoretical predictions: in theory, we expect the diffusion term \mathbf{g} to scale as $1/\sqrt{N}$ (see Equation 5).